## References

[1]Ibrahim, S. R., and Mikulcik, E. C., "A Method for the Direct Identification of Vibration Parameters from Free Response," *Shock and Vibration Bulletin*, No. 47, 1977, pp. 183–198.

[2]Ibrahim, S. R., "An Upper Hessenberg Sparse Matrix Algorithm for Modal Identification on Minicomputers," *Journal of Sound and Vibration*, Vol. 113, No. 1, 1987, pp. 47–55.

[3]Vold, H., Kundrat, J., Rocklin, G. T., and Russell, R., "A Multi-input Modal Estimation Algorithm for Minicomputers," SAE Paper 820194, 1982.

[4]Juang, J. N., and Pappa, R. S., "An Eigensystem Realization Algorithm for Modal Parameter Identification and Model Reduction," *Journal of Guidance, Control, and Dynamics*, Vol. 8, No. 5, 1985, pp. 620–627.

[5]Tasker, F., and Chopra, I., "Modified Sparse Time Domain Technique for Rotor Stability Testing," *Journal of Guidance, Control, and Dynamics*, Vol. 15, No. 6, 1992, pp. 1366–1374.

[6]Cherng, A. P., "Identification of Pseudo Stationary Modal Parameters—Updating and Detection," Ph.D. Dissertation, Department of Mechanical Engineering, Univ. of Maryland—UMBC, Jan. 1993.


# Modeling and Simulation of Rotor Bearing Friction


Arun K. Banerjee*
*Lockheed Palo Alto Research Laboratory, Palo Alto, California 94304*
and
Thomas R. Kane†
*Stanford University, Stanford, California 94305*


## Introduction

MODELING of friction is an important subject in all situations involving contacting surfaces, and various friction models exist in the literature.[1–4] Reference 2 evaluated several such models and came to the conclusion that all models except the classical Coulomb model simulated equally well motion under friction observed experimentally. This paper revisits four ways of modeling friction in bearings and examines these in the context of simulation of motion of a simple system, namely, a compound pendulum (a payload) supported by a journal bearing. The friction models considered are Coulomb friction, Dahl friction, and two friction models not considered in Ref. 2, namely, the friction circle model[5] and viscous friction. It is shown that a realistic treatment of Coulomb friction[6] in a rotor bearing requires the consideration of a two-degree-of-freedom model and the formulation of three sets of dynamical equations, one valid for slipping, one for sticking, and a third for transition from sticking to slipping. The other three friction models do not require such complex modeling and give rise to simpler simulations. The price of such simplicity, as numerical results show, however, is that, even though the motion of the pendulum predicted by all friction models is essentially the same, none of the models except the Coulomb model provides the detailed information on high-frequency chatter and the stick-slip nature of the motion.

## Journal Bearing Friction: An Example

A pendulum with friction at its hinge provides a simple system involving rotor bearing friction. Figure 1 shows a compound pendulum $B$ mounted in a bearing, with points $O$ and $O'$ being, respectively, the centers of the bearing and the journal, the bearing clearance having been exaggerated for the sake of clarity. The pendulum is of mass $m$ and centroidal inertia $J$, the journal radius is $r$ and the bearing radius $R$; and the distance from $O'$ to $B^*$, the mass center of $B$, is $L$ along the unit vector $\bar{b}_1$.

Received Oct. 6, 1993; revision received Dec. 21, 1993; accepted for publication Jan. 3, 1994. 

*Senior Staff Engineer. Associate Fellow AIAA.
†Emeritus Professor, Division of Applied Mechanics.

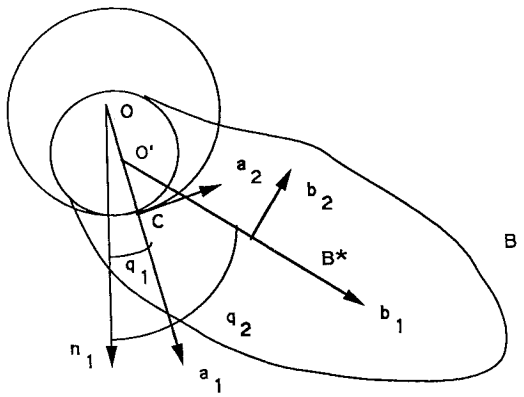


**Fig. 1 Compound pendulum mounted in rotor bearing.**

## Coulomb Friction Model

A fundamental fact that has not received sufficient attention in the literature on bearing dynamics is that simple rotation of a rigid body attached to a journal rotating in a bearing gives rise to a two-degree-of-freedom problem. This is illustrated in Fig. 1, where the journal, which is a part of $B$, contacts the bearing at point $C$. The angles $q_1$ and $q_2$ that the lines $OC$ and $O'B^*$ make, respectively, with a line fixed in the inertial frame characterize the two degrees of freedom of $B$. Coulomb's law of friction states that friction at the contact point $C$ prevents the bodies from sliding so long as the tangential force at $C$ does not exceed $\mu_s N$, where $\mu_s$ is the static coefficient of friction and $N$ is the normal force; once sliding occurs, the friction force $\bar{\tau}$ is described by

$$\bar{\tau} = -\mu_k N \frac{\bar{v}^C}{|\bar{v}^C|} \tag{1}$$

where $\mu_k$ is the kinetic coefficient of friction and $\bar{v}^C$ is the velocity of the point $C$ of $B$ that is in contact with the bearing. The equations of motion of the pendulum during sliding are

$$m[(R-r)\ddot{q}_1 + L\ddot{q}_2\cos(q_2-q_1) - L\dot{q}_2^2\sin(q_2-q_1) + g\sin q_1] = -\mu_k N \operatorname{sign}[(R-r)\dot{q}_1 + r\dot{q}_2] \tag{2}$$

$$mL[(R-r)\ddot{q}_1\cos(q_2-q_1) + L\ddot{q}_2 + (R-r)\dot{q}_1^2\sin(q_2-q_1) + gL\sin q_2] + J\ddot{q}_2 = -\mu_k rN \operatorname{sign}[(R-r)\dot{q}_1 + r\dot{q}_2] \tag{3}$$

where $N$, the normal reaction at the contact point, is given by

$$N = m[(R-r)\dot{q}_1^2 + L\ddot{q}_2\sin(q_2-q_1) + L\dot{q}_2^2\cos(q_2-q_1) + g\cos q_1] \tag{4}$$

Sliding gives way to rolling when the velocity of the contact point is equal to zero, in which event

$$(R-r)\dot{q}_1 + r\dot{q}_2 = 0 \tag{5}$$

In numerical simulations, the zero on the right-hand side of Eq. (5) is replaced by $\epsilon_1$, a small number chosen arbitrarily. With rolling, the number of degrees of freedom of the system is reduced to 1, and the equation of motion becomes

$$\{m[r^2 - 2rL\cos(q_2-q_1) + L^2] + J\}\ddot{q}_2 = -\frac{R}{R-r}mrL\dot{q}_2^2\sin(q_2-q_1) + mg(r\sin q_1 - L\sin q_2) \tag{6}$$

This equation is valid so long as the tangential force at the contact point is smaller than the static friction force. For the pendulum supported by the bearing, this condition is expressed as

$$|m(\bar{a}^{B^*} - g\bar{n}_1)\cdot\bar{a}_2| \le \mu_s N \tag{7}$$

where $\bar{a}^{B^*}$ is the acceleration of $B^*$, $g$ is the acceleration due to gravity, $\bar{a}_2$ is a unit vector parallel to the tangent to the contact

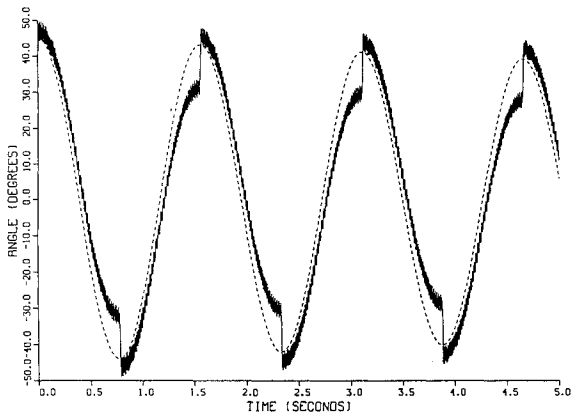


**Fig. 2 Time history of contact angle $q_1$ and pendulum angle $q_2$ with Coulomb friction model. Solid curve shows slipping, sticking, and transition at contact point.**

surface at $C$ (see Fig. 1), and $N$ is the normal reaction. In explicit form, the requirement (7) becomes

$$|[-r + L\cos(q_2 - q_1)]\ddot{q}_2 - L\dot{q}_2^2 \sin(q_2 - q_1) + g\sin q_1|$$
$$\leq \mu_s\left[\frac{r^2\dot{q}_2^2}{R-r} + L\ddot{q}_2\sin(q_2 - q_1) + L\dot{q}_2^2\cos(q_2 - q_1)\right.$$
$$\left. + g\cos q_1\right] \tag{8}$$

When the inequality (8) is violated, sliding begins. However, the numerical continuation of the simulation of motion is impeded by the fact that the velocity of the contact point at the end of rolling is zero, so that Eq. (1) ceases to be applicable. This difficulty is overcome by the following model of friction during the transition to slipping[6]: Since the direction of the friction force is known at the end of rolling, the friction force at the beginning of slipping is taken as having this direction and the magnitude $\mu_k N$. Accordingly,

$$F = -\mu_k N\ \text{sign}\left[(\bar{a}^{B^*} - g\bar{n}_1)\cdot\bar{a}_2\right] \tag{9}$$

where $\bar{a}^{B^*}$ is the acceleration of $B^*$ at the instant that Eq. (8) is violated. The equations of motion are the same as Eqs. (2) and (3), except that the argument of the sign functions in Eqs. (2) and (3) are replaced by that in Eq. (9). These transition equations are valid until

$$(R - r)\dot{q}_1 + r\dot{q}_2 = \epsilon_2, \qquad \epsilon_2 > \epsilon_1 \tag{10}$$

where, like $\epsilon_1$, $\epsilon_2$ is a small number chosen arbitrarily.

Numerical integration of the equations of motion was performed with the following parameter values and initial conditions: $r = 1$ in., $R = 1.002$ in., $L = 20$ in., $mg = 10$ lb, $J = 1$ lb-in.-s$^2$, $\mu_k = 0.13$, $\mu_s = 0.15$, $\epsilon_1 = 0.005$, $\epsilon_2 = 0.025$; $q_1 = 0$, $q_2 = 45$ deg, $\dot{q}_1 = \dot{q}_2 = 0$. The solid line in Fig. 2 is a plot of $q_1$, and the dashed line of $q_2$, vs time. From this figure, it is clear that the contact angle $q_1$ changes at a high frequency and that there is sticking at the interface between the bearing and the journal at the end of each swing of the pendulum, that is, whenever the sliding speed approaches zero. The behavior of $q_2$ is characteristic of the response of a pendulum subject to dissipative forces. The high-frequency behavior of $q_1$, which seems to be a new result, may explain the pitting and fatigue of bearings that are known to occur even under loads that vary slowly. Finally, it is noted in Fig. 2 that rolling occurs briefly at the end of each swing of the pendulum. Additional simulations revealed that, as the ratio of the bearing radius to the journal radius, $R/r$, increases, rolling of longer duration becomes possible in the presence of sufficient friction.

## Dahl Friction Model

As modeled by Dahl,[4] the effect of friction forces on the journal is represented, without any reference to a contact point, by a torque $\tau$ due to a couple acting to retard rotational motion. For a pendulum

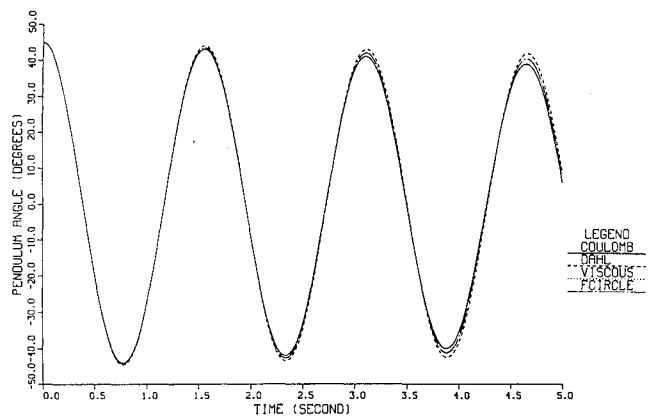


**Fig. 3 Pendulum motion as given by Coulomb, Dahl, friction circle, and viscous friction models.**

whose motion is characterized by a single rotational coordinate $q$, the equation of motion is

$$[mL^2 + J]\ddot{q} + mgL\sin q = -\tau \tag{11}$$

where $\tau$, in accordance with the Dahl friction model, is given by

$$\dot{\tau} = \gamma\dot{q}\left(1 - \frac{\tau}{\tau_s}\frac{\dot{q}}{|\dot{q}|}\right)^2 \tag{12}$$

where $\gamma$ and $\tau_s$ are two experimentally determined parameters. In Fig. 3 a plot marked with dashed lines corresponds to the solution of Eqs. (11) and (12) for $\gamma = 10^5$ in.-lb/rad and $\tau_s = 0.8$ in.-lb. As can be seen, the $q$-vs-$t$ curve describing pendulum motion for the Dahl friction model is essentially the same as that for the Coulomb model.

## Friction Circle Concept

According to the friction circle concept,[5] the total moment of all friction forces about the center of the journal is the negative of the moment of a certain force $\bar{R}$ that is applied to the journal tangentially at a point of a circle of radius $\mu_k r$, where $\mu_k$ is the kinetic coefficient of friction and $r$ is the radius of the journal. In the present situation, the force $\bar{R}$ is the resultant of the gravitational and inertia forces, so that

$$\bar{R} = m(L\dot{q}^2 + g\cos q)\bar{b}_1 - m(L\ddot{q} + g\sin q)\bar{b}_2 \tag{13}$$

and the associated differential equation of motion of the pendulum is

$$(mL^2 + J)\ddot{q} + mgL\sin q + \mu_k rm[(L\ddot{q} + g\sin q)^2$$
$$+ (L\dot{q}^2 + g\cos q)^2]^{0.5}\frac{\dot{q}}{|\dot{q}|} = 0 \tag{14}$$

In Fig. 3, the $q$-vs-$t$ curve representing pendulum motion corresponding to this approach with $\mu_k = 0.13$ is marked with lines broken by dots. Once again, we have the usual damped motion time history.

## Viscous Friction

If a thick fluid fim separates the rotor from its bearing, a description of the shearing action of the lubricant on the rotor is obtained by solving the Reynolds equation in the theory of hydrodynamic lubrication. Solutions of the Reynolds equation indicate[7] the existence of a power law between the coefficient of friction $\mu$ and the speed of rotation $\dot{q}$, and the equation of motion becomes

$$(mL^2 + J)\ddot{q} + \left(\frac{R}{R-r}\right)^{2k-1}\left(\frac{\nu w d\dot{q}}{N}\right)^k Nr\frac{\dot{q}}{|\dot{q}|}$$
$$+ mgL\sin q = 0, \qquad 0.7 < k < 1 \tag{15}$$

$$N = m(L\dot{q}^2 + g\cos q) \tag{16}$$

Equation (15), in which $\nu$ is the kinematic viscosity and w is the width of the bearing, reduces, for $k = 1$, to the form generally associated with viscous friction:

$$(mL^2 + J)\ddot{q} + c\dot{q} + mgL\sin q = 0 \tag{17}$$

The solution of Eq. (17) for $c = 0.5$ is included in Fig. 3 as a curve marked with a series of dots. We find that the motion of the pendulum as described by any one of the three complex friction models previously considered is essentially reproduced by the simple model of viscous friction.

## Conclusion

We have briefly reviewed four ways of modeling friction in bearings, namely, the Coulomb model, Dahl model, friction circle model, and viscous friction model. Although only Coulomb friction requires the consideration of a two-degree-of-freedom model, it is clear that this gives a richness of detail on stick-slip motion at the contact point that is not given by the other friction models, even though the gross motion of the rotor is reproduced equally well by all four models. Coulomb friction requires three sets of differential equations of motion corresponding to a single contact point, one for sliding, one for sticking, and a third for the transition from sticking to slipping. When friction must be considered at many bearings in a system, a simpler friction model may be preferred.

## References

[1]Rabinowicz, E., *Friction and Wear of Materials*, Wiley, New York, 1965.

[2]Haessig, D. A., and Friedland, B., "On the Modeling and Simulation of Friction," *Journal of Dynamic Systems, Measurement, and Control*, Sept. 1991, pp. 354–362.

[3]Karnopp, D., "Computer Simulation of Stick-Slip Friction in Mechanical Dynamic Systems," *ASME Journal of Dynamic Systems, Measurement, and Control*, Vol. 107, 1985, pp. 100–103.

[4]Dahl, P. R., "Solid Friction Damping of Mechanical Vibrations," *AIAA Journal*, Dec. 1976, pp. 1675–1682.

[5]Baumeister, T., Avallone, E.A., and Baumeister, T., III (eds.), *Marks' Mechanical Engineers Handbook*, McGraw-Hill, New York, 1978.

[6]Kane, T. R., and Levinson, D. A., "A Realistic Solution of the Symmetric Top Problem," *Journal of Applied Mechanics*, Vol. 45, No. 4, 1978, pp. 903–909.

[7]Shigley, J. E., and Mischke, C. R., *Mechanical Engineering Design*, McGraw-Hill, New York, 1989.

# Comparative Stability Study Illustrating Advantages of Guy-Wire Constraints for Flexible Satellites

A. P. Mazzoleni*
*Texas Christian University, Fort Worth, Texas 76129*
and
A. L. Schlack†
*University of Wisconsin, Madison, Wisconsin 53706*

## Introduction

SINCE the beginning of the space age much attention has been given to the control and stability of artificial satellites. In the 1960s and 1970s many passive methods of stabilization were studied. (By passive we mean without the use of a control system. Gravity-gradient, spin-stabilized, and dual-spin satellites are examples of satellites stabilized by "passive" means.) As time went on, however, more and more attention was given to active control of satellites and the interest in passive means of stabilization declined. It is proposed here that an important passive means of attitude stabilization has not been fully exploited, namely the use of guy wires to improve the stability of flexible satellites.

Presented as Paper 92-154 at the AAS/AIAA Space Flight Mechanics Conference, Colorado Springs, CO, Feb. 24–26, 1992; received April 17, 1993; revision received Nov. 1, 1993; accepted for publication Nov. 5, 1993.

*Department of Engineering. Member AIAA.
†Department of Engineering Mechanics. Member AIAA.

The need for another means of passive stabilization may not seem obvious due to the fact that control technology has evolved to the point where satellites are routinely controlled to high degrees of pointing accuracy. The advantage in designing a satellite that is inherently stable in its uncontrolled state lies in the fact that the power required to control such a satellite is much less than the power required to control a more unstable satellite. This will become increasingly important in the future as large space structures that are extremely flexible are built.

Previous studies by the authors[1,2] have shown that stability for gravity-gradient-stabilized and dual-spin-stabilized satellites can be achieved over a wide range of parameter values when guy-wire constraints are used to constrain vibrations of flexible appendages to torsional modes. This suggests that guy-wire constraints are a promising lightweight method of increasing satellite stability. In order to determine the extent of the benefits to be gained by using guy-wire constraints in satellite design, however, it is necessary to have a comparison of the stability conditions for a satellite model with and without guy wires. This paper provides a comparative study of stability conditions for Earth-pointing, dual-spin and gravity-gradient satellites, with and without guy wires.

## Satellite Model

The unconstrained satellite model consists of a dual-spin, Earth-pointing, flexible satellite in a circular orbit about a spherically symmetric planet. The satellite model, shown in Fig. 1, consists of a central body containing an internal rotor and two rectangular solar panels supported by elastic, massless beams. The central body, rotor, and panels are assumed to be rigid. Each supporting beam has length $L$, principal torsional stiffness $D_\xi$, and principal flexural stiffnesses $D_\zeta$ and $D_\eta$. The masses of the central body, rotor, and panels are denoted by $M_c$, $m_r$, and $m_p$, respectively. The central body has principal body axes $\boldsymbol{i}, \boldsymbol{j}, \boldsymbol{k}$, which are also principal body axes for the entire satellite in its undeformed state. The origin $O$ of the $\boldsymbol{i}, \boldsymbol{j}, \boldsymbol{k}$ coordinate system is the center of mass of the central body and the center of mass of the entire undeformed satellite. The principal moments of inertia of the central body about the axes $\boldsymbol{i}$, $\boldsymbol{j}$, $\boldsymbol{k}$ are denoted $A_c$, $B_c$, and $C_c$. The center of mass of the rotor is located at $O$ and the rotor spins about the $\boldsymbol{k}$ axis at a constant rate $\omega_s$ relative to the central body. The principal moments of inertia of the rotor about the axes $\boldsymbol{i}, \boldsymbol{j}, \boldsymbol{k}$ are denoted $A_r$, $B_r$, and $C_r$. Because the rotor is axially symmetric, $A_r = B_r$. The principal moments of inertia of the panels about their principal axes are denoted $A_p$, $B_p$, and $C_p$ and the principal axes of the panels are aligned with the axes $\boldsymbol{i}, \boldsymbol{j}, \boldsymbol{k}$, as shown in Fig. 1.

Because the beams are elastic, they can flex and twist if the satellite is disturbed. To describe the kinematics of such a deformation, we follow the method developed by Crespo da Silva and Glynn[3] as detailed in Ref. 4. Consider, for example, the right beam of the satellite in Fig. 1. In general, each cross section of the beam can experience an elastic displacement of its centroid and a rotation about its centroid. Therefore, three generalized coordinates are needed to describe the elastic displacement of the cross section and three generalized coordinates are needed to describe the rotation of the centroid. We now describe the kinematic notation of the beam (Fig. 2). Let $s$ denote the arc length of the beam. Then, we denote the components of the elastic displacement vector of the centroid, at an arbitrary location $s$ along the $\boldsymbol{i}, \boldsymbol{j}, \boldsymbol{k}$ axes, by $x_R(s)$, $y_R(s)$, and $z_R(s)$, respectively. To describe the rotations, a coordinate system $\zeta_2(s)$, $\xi_2(s)$, $\eta_2(s)$ is embedded in the beam at each position $s$. In

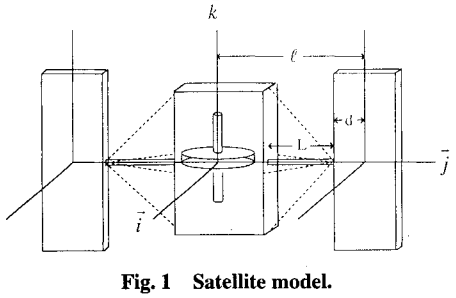


**Fig. 1 Satellite model.**